17th World Conference on Earthquake Engineering, 17WCEE
Sendai, Japan - September 13th to 18th 2020

RUPTURE MODELING FOR THE 2016 KUMAMOTO, JAPAN AND 2019 RIDGECREST CALIFORNIA EARTHQUAKES

A. Pitarka[1], H. Kawase[2], R. Graves[3], K. Miyakoshi[4], L. Dalguer[5], K. Irikura[6], A. Rodgers[7], D. McCallen[8]

[1] *Seismologist, Lawrence Livermore National Laboratory, pitarka1@llnl.gov*
[2] *Program-Specific Professor, DPRI, Kyoto University, JAPAN, kawase@sere.dpri.kyoto-u.ac.jp*
[3] *Seismologist, United States Geological Survey, Pasadena, CA, rwgraves@usgs.gov*
[4] *Geophysicist, Georesearch Institute, Osaka, Japan, ken@geor.or.jp*
[5] *Earthquake Engineer, 3Q-Lab, Switzerland, luis.dalguer@gmail.com*
[6] *Professor, Aichi Institute of Technology, Toyota, Japan, irikura@geor.or.jp*
[7] *Seismologist, Lawrence Livermore National Laboratory, rodgers7@llnl.gov*
[8] *Professor and Director of the Center for Civil Engineering Earthquake Research, University of Nevada, Reno and Senior Scientist, Lawrence Berkeley National Laboratory, dmccallen@unr.edu*

Abstract

The M7.1 2019 Ridgecrest, California and M7, 2016 Kumamoto, Japan earthquakes produced high quality ground motion data that are very important for studying crustal earthquakes that rupture to the surface. Both earthquakes are predominantly strike slip events. They have similar fault dimensions, and large-scale slip variations with similar characteristics. The main objective of our study is the characterization of rupture models for each fault, and investigation of similarities in the rupture process and ground motion variability, through comparisons between simulated and observed near-fault ground motions. First, we performed rupture dynamics modeling to constrain shallow slip characterization in rupture models for crustal earthquakes. The simulations of spontaneous rupture were performed in the frequency range 0-2.0Hz, using a 3D staggered-grid finite-difference method and a layer over half-space 1D crustal velocity model with a minimum shear-wave velocity of 2.8 km/s. In order to account for changes in material ductility and reduction of stress drop, observed in the shallow crust (upper 3-5 km), and the transition from ductile state to brittle state in the upper seismogenic zone, in our stress models we included a shallow weak zone (<4km). In this zone the stress drop was set to zero at the free surface and gradualy increased with depth, while the slip weakening distance was set to 100 cm at the free surface and decreased to 40 cm at the base of the weak zone. From these computations we found a systematic change in the shape of the slip-rate function from Kostrov-like in the deeper part of the fault to more symmetric in the upper few km near the free-surface. Moreover, the average slip duration in the weak zone, with respect to slip duration in the deeper parts of the fault, increases by at most a factor of 2. The simulations also indicate that, due to weak zone effects, the contribution of near-free-surface fault rupture to generated sesimic energy is reduced in the intermediate frequency range 0.3-1Hz. Then for each earthquake the observed slip distribution was used as a reference in selecting rupture models generated with the GP method [1]. Constrained by the observed slip distribution and consistent with dynamic rupture models, the rupture models of both earthquakes contain areas with relatively large slip rate, representing strong motion generation areas, set against lower amplitude heterogeneous background slip, and a relatively low slip rate in the weak zone of the top-most crust (upper 4km). Finally, we analyzed the sensitivity of computed near-fault broad-band (0-10Hz) ground motion characteristics, including ground motion amplitude, velocity pulse and spectral response, to strong motion generation areas, and investigated similarities and dissimilarities between the two earthquakes. For example, in the case of Ridgecrest earthquake, we found that slip models with large slip patches reaching the free surface produce ground motion with correct amplitude in the intermediate frequency range (0.3-1 Hz), compared to models with buried slip patches. The results of our study suggest that in order to correctly reproduce the observed reduction in the contribution of fault rupture to near-fault PGV and acceleration spectral responses in the intermediate frequency range, during crustal earthquakes on faults that break the free surface, proper care needs to be taken when representing shallow rupture kinemtics in strong ground mostion simulations. We conclude that the inclusion of depth dependent kinematic rupture characteristics improve the performance of hybrid rupture models of crustal earthquakes in reproducing the low and high frequency characteristics of recorded ground motion.

Keywords: Physics-based rupture models; rupture dynamics; kinematic rupture models; strong ground motion;2019 Ridgecrest earthquake

1. Introduction

Kinematic rupture models used in numerical predictions of ground motion should be tied to physical constraints on the causative source physics. The objective of our study is the improvement of shallow rupture characterization in kinematic rupture models used in strong ground motion simulations. Based on geological investigations, earthquake stress drop, depth-variation of seismicity, as well as recorded near-fault ground motion, there is clear evidence for depth variation of frictional properties of crustal materials. The material ductility in the weak zone (upper 3-5 km of the crust) and the transition from ductile state to brittle state in the upper seismogenic zone, determine how the fracture energy is consumed by the earthquake rupture, and how generated seismic energy is distributed in space and time.

Using plausible stress models for crustal ruptures, we performed dynamic rupture simulations on vertical strike slip faults that break the free surface. The stress drop was modeled using the linear slip weakening frictional law that reflects the depth and lateral variations of frictional properties of crustal materials. Through dynamic rupture modeling we were able to extract kinematic rupture characteristics, such as changes in the shape of slip rate functions, rupture velocity, and peak slip rate across the weak zone, and in the slip asperity areas. These results were then used to refine our existing rupture generating model [1] for crustal earthquakes. The modifications to the rupture generator code include changes to the shape of slip-rate function at shallow depths, rise time variation with depth and stronger correlation with slip at shallow depths.

The effects of the proposed characterization of shallow rupture kinematics on simulated ground motion was then investigated in broad-band (0-10Hz) simulations of the M7.1 2019 Ridgecrest California earthquake. The ground motion time histories were computed using the hybrid method of Graves and Pitarka [4]. In our simulations we considered several slip distributions, including models obtained by inverting recorded velocity and displacement ground motion. Finally, through comparisons with recorded data, for both Ridgecrest and Kumamoto earthquakes, we analyzed the sensitivity of computed near-fault broad-band ground motion characteristics, including the amplitude of velocity pulse, and response spectra, to shallow slip and location of strong motion generation areas (areas with high slip rate).

2. Dynamic Rupture Modeling

One of the key ingredients in the parameterization of material stress properties implemented in our dynamic rupture modeling is the inclusion of a weak zone in the shallow part of the model. By weak zone we mean a shallow layer of reduced dynamic stress drop resulting from low initial shear stress levels at shallow depth, and frictional properties distinct from those at deeper levels, or both. The weak zone is a layer of relatively incompetent fault gouge that is not able to maintain large shear stresses. A thick gouge layer may also have frictional behavior in which the resisting force during sliding increases with the slip velocity. Studies of shallow post seismic slip of large earthquakes [5] provide indirect evidence for a velocity-strengthening fault rheology at shallow depths.

Pitarka et al. [6], and Dalguer et al. [7] discuss the physical properties of the shallow-weak layer and simulate its effects in reducing high-frequency seismic energy, enhancing long period energy, and reducing rupture speed during shallow faulting. Using the concept of the weak zone Pitarka et al. [6] performed numerical simulations of rupture dynamics with depth dependent frictional properties to explain the frequency-dependent difference between observed ground motion from buried and surface rupturing. In this study we pursue the concept of shallow weak-layer effect on surface-rupture dynamics using models with stochastic stress drop, and examine the extent to which it affects the rupture kinematics, including spatial and temporal changes of slip rate function, slip, and rupture speed.

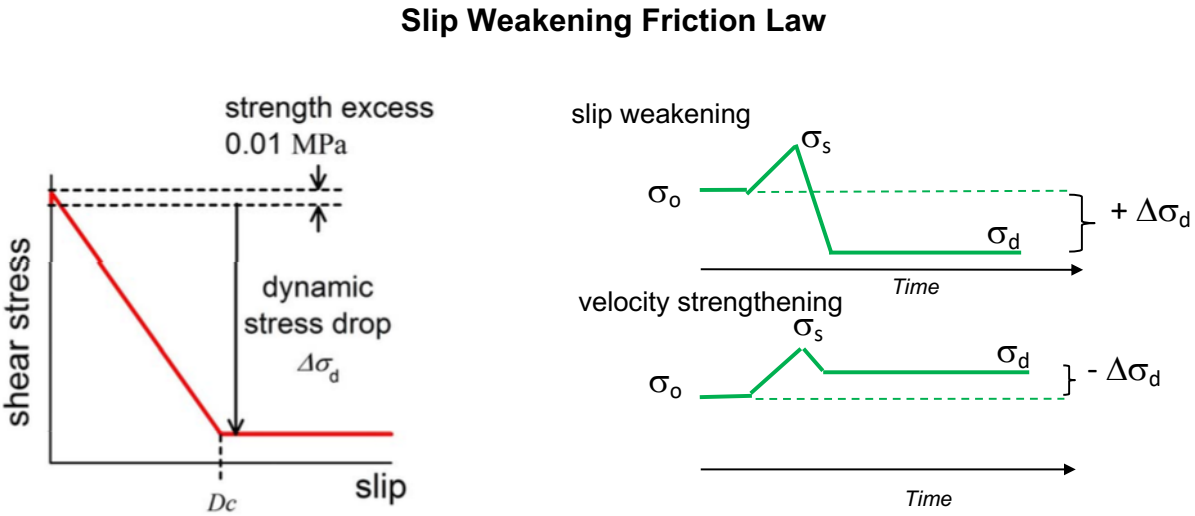

Fig. 1 - Linear slip weakening friction law (Andrews, 1976). The right panel illustrates stress evolution with time in areas with positive stress drop (slip weakening) , and areas with negative stress drop (equivalent to velocity strengthening in parts of the weak zone).

We adopted a stochastic characterization of the spatial complexity of earthquake rupture stress drop in which the stress distribution is described by a power spectral density function in the wavenumber domain, parameterized by two characteristic length scales, along the strike and dip directions, respectively. Both initial shear and normal stress in our models are considered variable in space, but they have the same spatial variation pattern. The static friction coefficient was selected based on the condition that the average value of S should be greater than 2. Under this condition all generated models produced rupture speeds that remain subshear over large areas, except for very small regions where low S may have increased the rupture speed to super-shear. The fault is a vertical plane embedded in a layered space. The rupture nucleates at a given location in a circular area within which we adjust the static friction coefficient so as to bring the strength excess (static shear strength minus initial shear stress) to zero. Figure 1 illustrates the linear slip weakening friction law adopted in our rupture modeling. The figure also illustrates the concept of positive stress drop in areas with large stress drop, and negative stress drop in parts of the shallow weak zone where the velocity strengthening occurs. Figure 2 shows the stress parameterization used in dynamic rupture modeling for a rupture with a weak zone. The fault rupture is 35x18 km, and it reaches the free surface. We used a 3D staggered-grid finite-difference method proposed by Pitarka [2] that uses the staggered grid split-node method of Dalguer and Day [3], and a 1D velocity model to performe rupture dynamics simulations. The finite-differnec grid spacing is 80 m which ensures a maximum modeled frequency of 2.0 Hz.

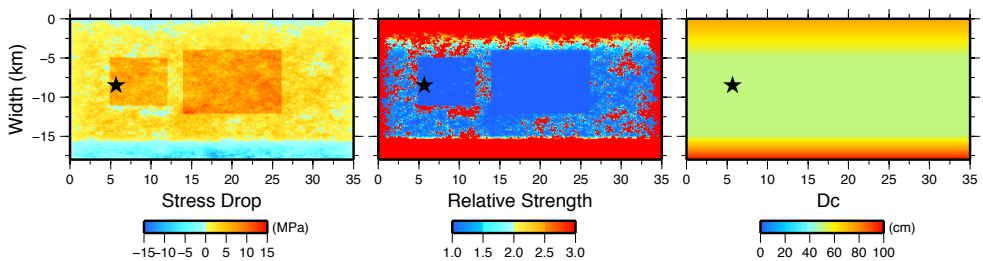

Fig. 2 - Stress parametrization used in rupture dynamics: Stress drop (left panel), Relative Fault Strength (middle panel) and slip weakening distance D_c (right panel)

3. Kinematic Rupture Characteristics Derived from Rupture Dynamics

The main products that we extracted from the rupture dynamics modeling are the slip rate time histories, slip and peak slip rate distributions, and rupture velocity. All are key parameters of rupture kinematics which control the spatial and temporal distribution of seismic energy released during the fault rupture. Figure 3 summarizes the slip characteristics obtained from our rupture dynamics modeling using the generic stress model illustrated in Figure 2. Figure 3a shows the distributions of computed final slip, peak slip rate, peak slip rate time (t_o), and rupture time on the fault plane. Slip rate time t_o is computed as the difference between the time of the peak slip rate, and the slip rate onset. As will be discussed subsequently, an area with relatively short t_o and high peak slip rate generates high frequency ground motion. In contrast, areas with relatively long t_o and low peak slip rate generate ground motions that are mostly dominated by long period energy (> 1s). Figure 3b illustrates time histories of the slip rate obtained from the dynamic rupture simulation at selected receivers located on the fault. S1, S2, and S3 are located in the weak zone, at a depth of 2.4 km. S4, S5, and S6 are located in high stress drop areas and S7, S8 and S9 are located in the background slip below the high stress drop areas, at a depth of 15 km. Vertical profiles of stress drop, permanent slip, peak slip rate, and slip rate function, across the two high stress drop patches, are shown in Figure 3c and 3d, respectively.

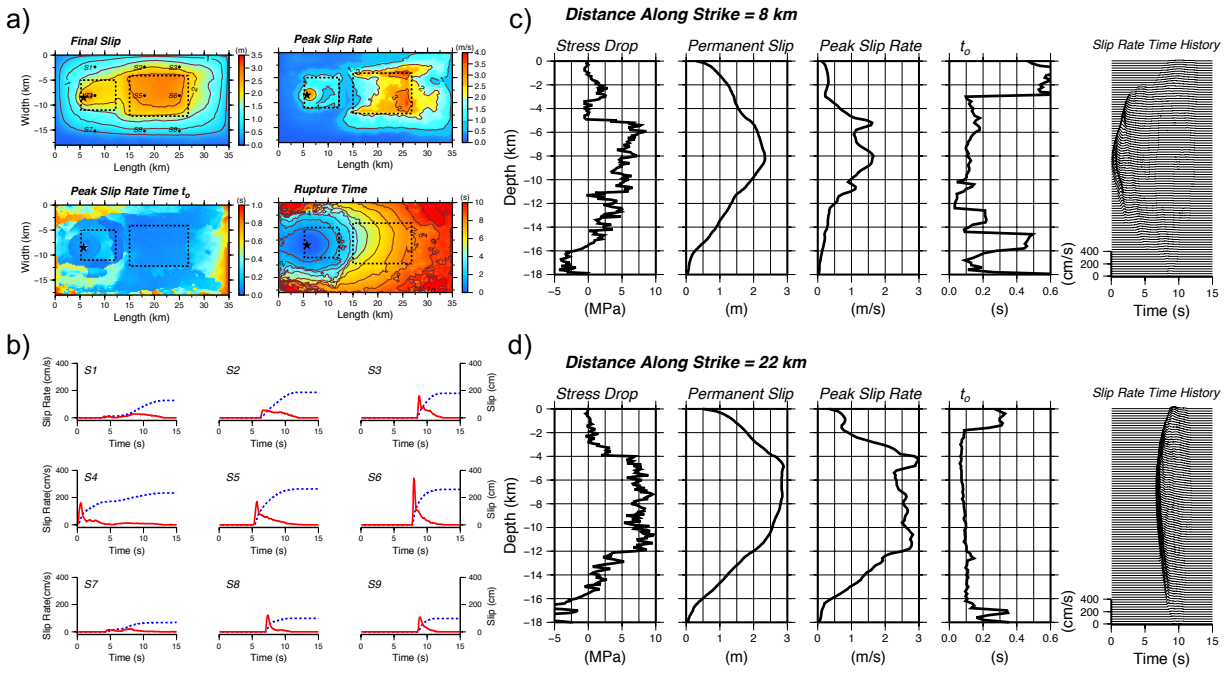

Fig. 3 - Kinematic slip derived from dynamic rupture modeling. a) Final slip, peak slip rate, peak slip rate time (t_o), and rupture time. b) Time histories of fault slip rate (red traces) and slip (blue traces) at different receivers. The receiver locations and names are indicated by black triangles on the final slip panel. c) Vertical profiles of stress drop, final slip, peak slip rate and slip rate time histories across two high stress drop areas, located at distances of 8km and 22km along the fault strike.

These results display several interesting rupture features. First, due to strong differences in material frictional properties and stress drop between the weak zone and high stress drop areas, the slip and slip velocity

are higher in and around the high stress drop areas, and lower in the top 3 km of the fault. Similarly, the peak slip rate and rupture velocity is high in the asperity areas and lower in the weak zone. The fault slip at the free surface is variable. It tends to be higher above the high stress drop areas. Second, as illustrated by the vertical profiles, and at selected receivers, the shape of the slip rate function varies significantly, especially with depth. In the high slip rate areas the slip rate function is of Kostrove-type, and has a very short t_o. In contrast, in the weak zone (upper 4 km) the shape of the slip rate function is roughly similar to a cosine function with often a relatively long t_o. In addition, the peak slip rate is much lower in the top and bottom weak zones. When the rupture penetrates into the weak zone, the rupture propagation decelerates, the slip rate gets smoother, and its peak is gradually reduced toward the free surface, but then at the free-surface, the peak slightly recovers due to the free-surface reflection. These weak zone effects on slip-rate function also cause the reduction of the high frequency ground motion originated from shallow slip. Third, due to rupture deceleration and delay of reflected pulses from the free surface and stopping phases from the fault edges, the rise time becomes longer in this zone, suggesting a shift to lower frequency content of the ground motion generated in the shallow part of the fault. Simulation results obtained with slightly different locations and sizes of large stress drop areas, and different rupture initiation locations, not shown here, display similar rupture kinematic trends, especially in the shallow part of the fault. Here we use these observations to refine our hybrid rupture generation method [1] for crustal earthquakes. The main modifications to our rupture generator GP include gradual changes to the shape of slip-rate function from Kostrov-type to cosine-type at shallow depths, and rise time variation with depth.

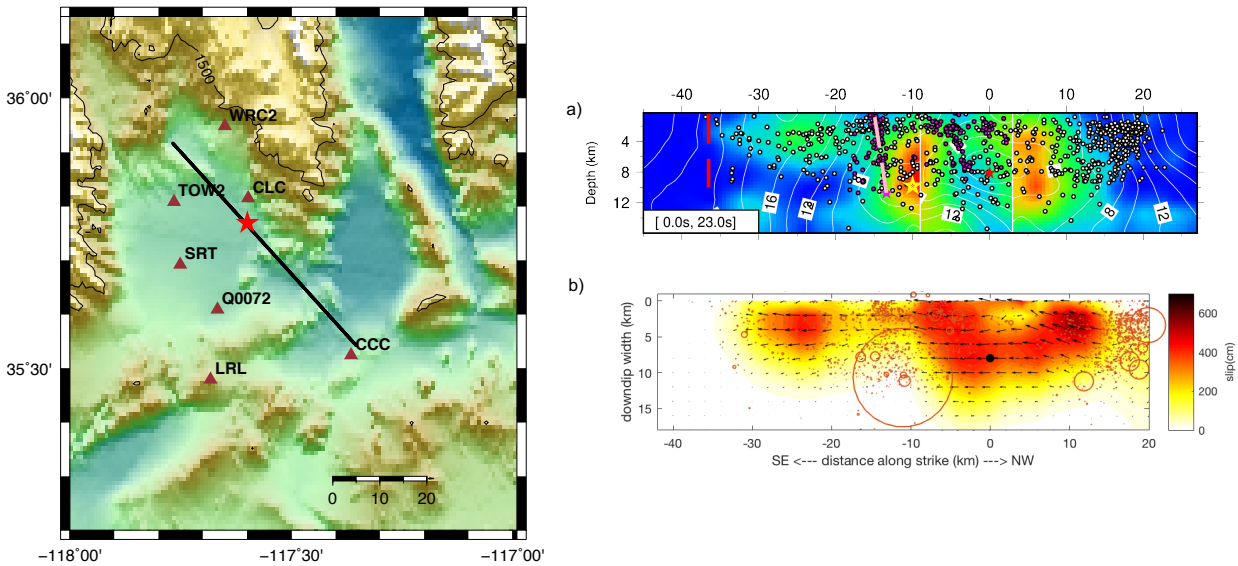

Fig. 4 - Left panel: Map of the study area showing the fault surface trace (black line), epicenter (red star) and strong motion stations (red triangles). Right panel: Slip models obtained from inverting ground motion data, proposed by Ji et al. [9] and Dreger et al. [8], a) and b), respectively. The circles in both panels indicate foreshocks and aftershocks.

4. Rupture Models and Simulations of the 2019 Ridgecrest Earthquake

We used the modified rupture generator to produce kinematic rupture models that were used in ground motion simulations of the M7.1 2019 Ridgecrest, California (USA) earthquake. The Ridgecrest earthquake occurred on a three segment predominantly strike-slip fault that ruptured to the free surface. The fault is part of the Eastern California Shear Zone (ECSZ), a seismically active region east of the southern segment of the San Andreas Fault (SAF) and largely coincident with the Mojave, featuring multiple right-lateral strike-slip faults

paralleling the SAF. In addition to the 2019 Ridgecrest earthquake sequence, several magnitude 7+ earthquakes have occurred along the eastern California shear zone, including the 1992 Landers earthquake, 1999 Hector Mine earthquake, as well as the massive 1872 Lone Pine earthquake in the Owens Valley.

The Ridgecrest earthquake was recorded at several strong motion stations. The closest station is located 2 km from the fault. We computed ground motion at seven near-fault stations (distance < 30 km). Most of the stations are located on hard soil conditions. The surface trace of the modeled rupture and the station locations are shown in Figure 4. Although surface expressions of the fault and aftershock distributions suggest that the earthquake ruptured three different fault segments, in this preliminary study the fault rupture was modeled by a single plane. Several source inversions using ground motion data have indicated that the fault rupture was dominated by at least three shallow large slip patches and had a relatively low rupture velocity, as low as 70% of the local Vs. Figure 4 shows two rupture models, Model 2 and Model 3, constrained by slip models proposed by Dreger et al. [8] and Ji et al. [9], respectively. The kinematic slip models proposed for the Ridgecrest earthquake were mainly used to constrain the size and location of large slip areas. The location and the size of the square-shaped slip patches in our model were based on an interpretation of large slip patches in the proposed kinematic slip models, so that each individual squared patch includes only areas of large slip in which slip is higher than 20% of the maximum slip.

Using comparisons between synthetic and recorded motion at near-fault stations, we investigated the impact of kinematic rupture models on simulated broad-band (0-10 Hz) ground motion. The simulations were performed with the technique of Graves and Pitarka [4] (GP) which combines deterministic and stochastic approaches in simulating the low (<1 Hz) and high frequency (>1 Hz) parts of ground motion, respectively. The GP method has been validated against recorded earthquakes as well as Ground Motion Prediction Equations (GMPES) for the Western US.

In addition to Model 2 and Model 3 we considered two rupture models that represent rupture scenarios that we would have selected to predict strong ground motion for a Ridgecrest-type earthquake rupture. In the first model (Model 0) the slip distribution is fully stochastic, and in the second model (Model 1) the slip is a combination of a large slip patch with a stochastic background slip. The rupture models are shown in Figure 5. Note that all models have a gradual decrease in peak slip rate at depths smaller than 4 km. This feature is expected to impact the frequency content of the slip rate and reduce the amount of high frequency energy released in the shallow part of the fault. Figure 6 shows the comparison between the recorded and simulated time histories of ground motion acceleration and velocity, low-pass filtered at 10 Hz. The simulated ground motions are corrected for site effects using Vs_{30} empirical site factors. Based on these comparisons, the general assessment of the simulations performance is that, except for station CCC, the considered rupture models perform satisfactorily. Station CCC is located near the southern edge of the fault. The ground motion at this station is very complex as it is affected by ground motion generated by two large slip areas, located north west of the rupture initiation, as well as the ground motion generated by a smaller slip area, located south east of the rupture initiation. At station CCC the observed complex wave packages and their arrival time is affected by backward and forward rupture directivity effects at this site. Such effects are generally difficult to predict by forward modeling as they are very sensitive to rupture details.

The performance of the rupture models in simulations was examined by using the goodness of fit plots, shown in Figure 7. These plots compare the bias of RotD50 pseudo spectral acceleration response with 5% damping (ln(Rec/Syn)) between recorded (Rec) and synthetic (Syn) ground motion, averaged over 7 stations. It is clear that between the four simulations the simulation based on Model 2 does a better job at fitting the recorded data. Similarly to rupture Model 1, dominated by a single large slip patch, ground motion computed with Model 3 is higher than the recorded one in the period range 1-3s. The main reason for this discrepancy is the relatively high slip in slip patches in both models. Slip patches with very high slip can increase the amplitude and shorten duration of computed ground motion velocity pulses, resulting in enhanced seismic energy in the intermediate period range (1-3s). The effect of weak zone in suppressing shallow slip is clear in

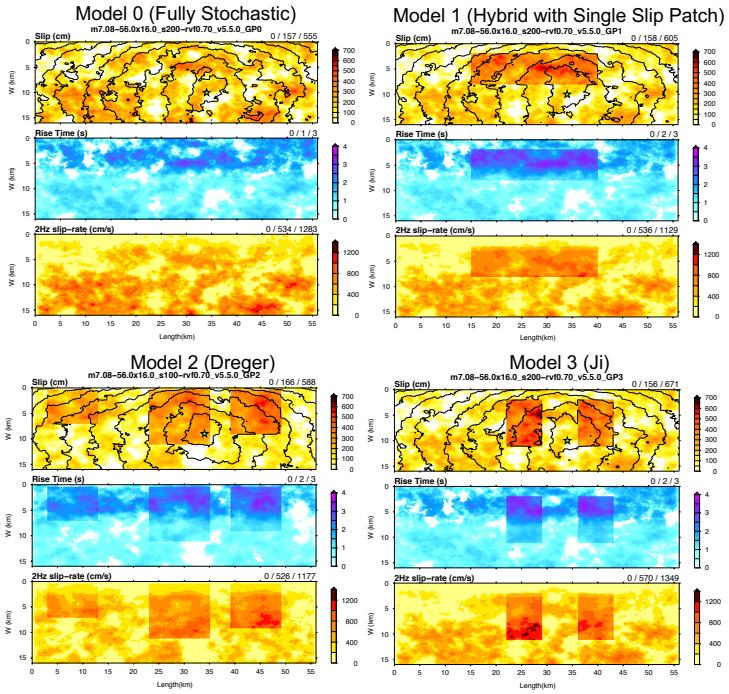

Fig. 5 - Rupture models used in ground motion simulations of the M7.1, 2019 Ridgecrest earthquake. The model names are indicated on top of each panel. The first row shows the slip distributions, the second row shows the rise time, and third row shows the peak slip rate computed after low-pass filtering the source time function at 2 Hz. The triplet of numbers at the upper right of each panel indicate the minimum, average and maximum values of the parameter being displayed. Isochrones indicate rupture front at 1 s time intervals.

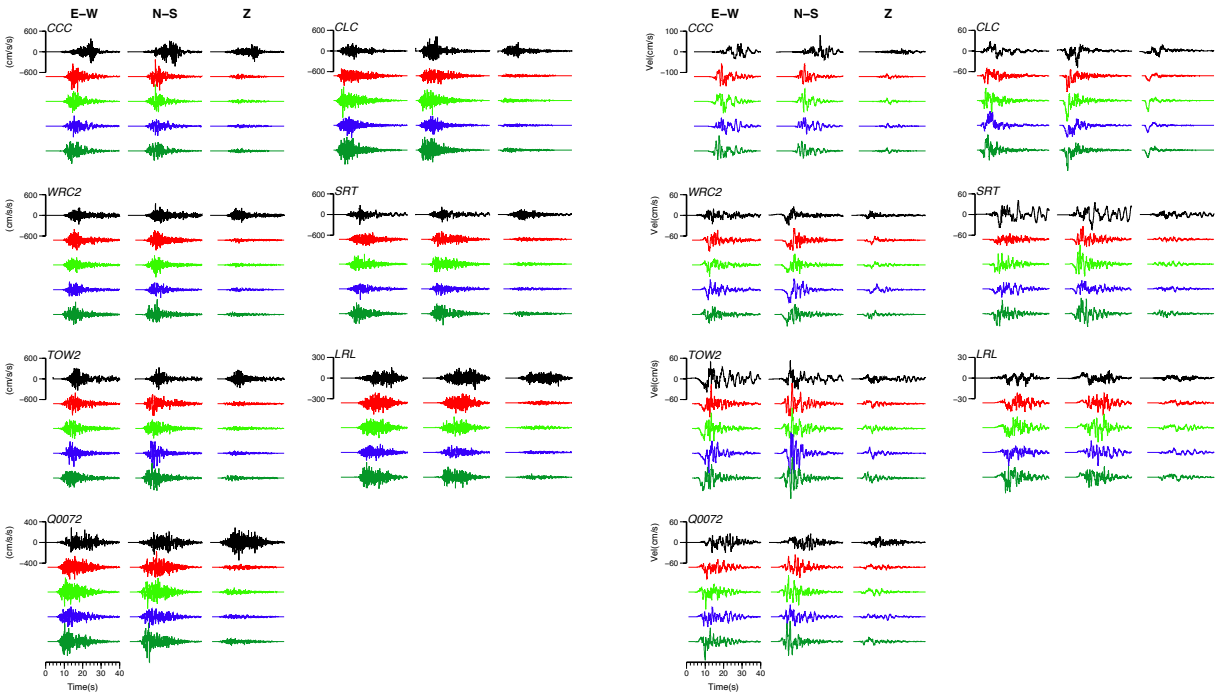

Fig. 6 - Comparison of recorded (black traces) and simulated (colored traces) ground motion acceleration (left panel) and velocity (right panel), low-pass filtered at 10 Hz.

the goodness of fit for Model 2 in which a large portion of the large slip patches penetrate in the weak zone. In this case the high-frequency portion of seismic energy radiated in the slip patches is relatively low.

The effects of slip distribution on simulated near-fault ground motion velocity is demonstrated in Figure 8. In this figure we compare the recorded and simulated ground motion velocity and RotD50 SA at station CLC which is the closest to the fault. The most significant differences between the recorded and simulated ground motions are seen for Model 1 and Model 3. Due to stronger local directivity effects these models produce ground motion with larger velocity pulses on both N-S and E-W components. In contrast, Model 2 produces ground motion that is similar to the recorded one. The slip in Model 2 is dominated by three large slip areas. Because a relatively larger portion of shallow slip in Model2 penetrates the weak zone, in contrast with those in Model 1 and Model 3, the seismic energy radiated by the large slip areas is lower, especially in the intermediate period range 1-3s. This is clearly seen in the plots of RotD50 spectral acceleration response. In conclusion, Model 2 produces ground motion which overall better fits the observed velocity pules and spectral response.

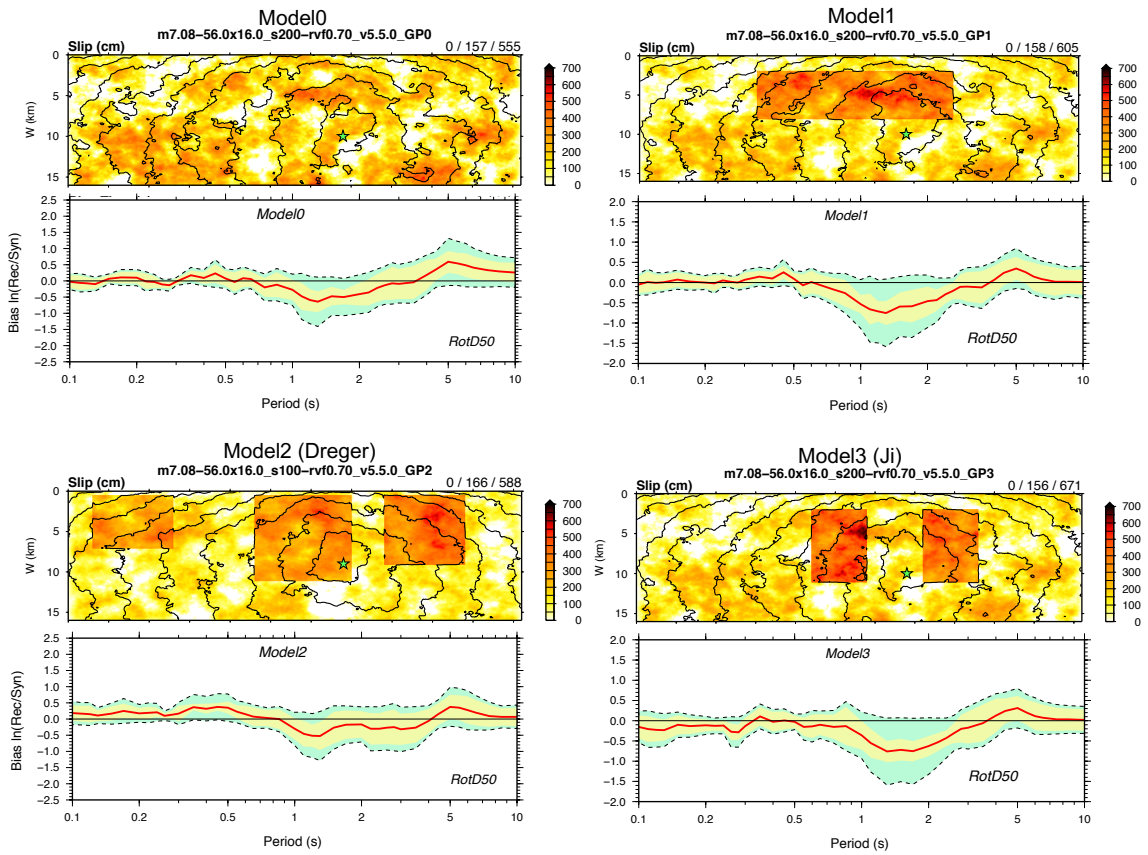

Fig. 7 - Rupture models and spectral acceleration goodness of fit, averaged over 7 stations used in ground motion simulations of the Ridgecrest earthquake. The model names are indicated on top of each panel. The first row shows the slip distributions. The triplet of numbers at the upper right of each panel indicate the minimum, average and maximum values of the slip. Isochrones indicate the rupture front at 1 s time intervals. The second row shows RotD50 horizontal spectral acceleration goodness of fit for the simulations. The residuals used in the goodness of fit are computed between the simulated and the recorded data

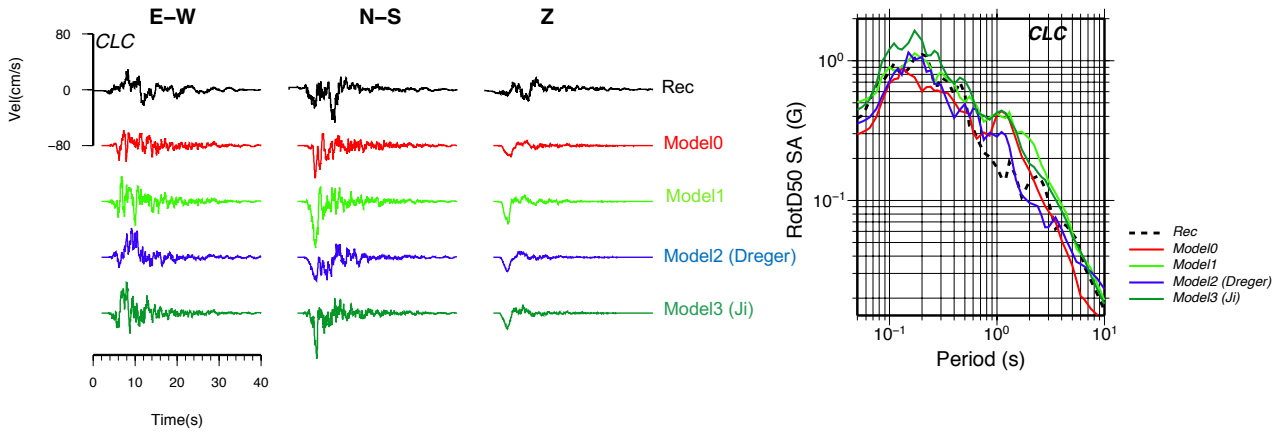

Fig. 8 - Recorded (black traces) and simulated (colored traces) ground motion velocity at station CLC. Left panel shows the comparison of the corresponding RotD50 spectral accelerations.

5. Strong Ground Motion Simulation of the 2016 Kumamoto Earthquake

The performance of the hybrid rupture generator was also examined in near-fault ground motion simulations for the M7, 2016 Kumamoto Japan earthquake performed by Pitarka et al. [10]. The Kumamoto earthquake is a strike slip event that ruptured four fault segments. Figure 9 shows the location of the fault segments and strong motion stations used in ground motion simulations. Similarly to the Ridgecrest earthquake, the earthquake rupture reached the surface, and was dominated by three shallow large slip areas. In analysis of shallow rupture characteristics Pitarka et al. [10] performed BB simulations using selected hybrid rupture models containing both, discrete high-slip patches following the Irikura recipe, and shorter length-scale spatial and temporal heterogeneities. Two rupture models, one with stochastic slip (model GP) and the other one with large slip patches (model HB2) used in their analysis are shown in Figure 9. The rupture kinematics in these models include depth-dependent features that reflect the weak zone effects, as described in this study. Figure 9 also shows a synthesis of the simulations' performance represented by the bias of RotD50 pseudo spectral acceleration response with 5% damping, averaged over 19 stations. Overall the bias obtained with the two models is small in a broad frequency range (0–10 Hz). It was found that a depth dependent of slip-rate function with a shorter rise time in areas below the weak zone, as well as faster rupture speed in the high stress drop areas, is necessary to reproduce both the low and high frequency characteristics of recorded ground motion.

6. Conclusion

Simulation of rupture dynamics on vertical faults that rupture the free surface were used to extract kinematic rupture characteristics that inherit weak zone effects on shallow slip, observed during crustal earthquakes. In addition to systematic changes in peak slip rate and rupture velocity, from these simulations we found a systematic change in the shape of the slip-rate function from Kostrov-like on the deeper fault to more symmetric in the upper few km near the free-surface. Moreover, the average slip duration in the weak zone, with respect to slip duration in the deeper parts of the fault, increases by at most a factor of 2. The simulation results also indicate that the weak zone reduces the seismic energy generated by the shallow slip, in the intermediate frequency range 0.3-1Hz. The new rupture kinematics were used to improve the parameterization of our GP rupture generating technique. The modifications include depth-dependent shape of the slip-rate function, rise time, and rupture speed, with stronger correlation with slip.

The effects of the proposed characterization of shallow rupture kinematics on simulated ground motion was then investigated in broad-band (0-10Hz) simulations of the M7.1 2019 Ridgecrest California and M7 Kumamoto, Japan earthquakes. Specifically, in these analyses we examined the impacts of longer rise time and lower rupture speed in the shallow weak zone, and shorter rise time and faster rupture speed in the high stress drop regions (strong motion generation areas). We found that rupture models that better fit the observed ground motion for both Ridgecrest and Kumamoto earthquakes include strong motion generation areas that are located below the weak zone, and shallow slip with a relatively long duration. Based on modeling of dynamic fault rupture in crustal materials with heterogeneous properties, and ground motion simulations of both earthquakes, we conclude that the inclusion of depth dependent kinematic rupture characteristics improve the performance of hybrid rupture models of crustal earthquakes in reproducing the low and high frequency characteristics of recorded ground motion.

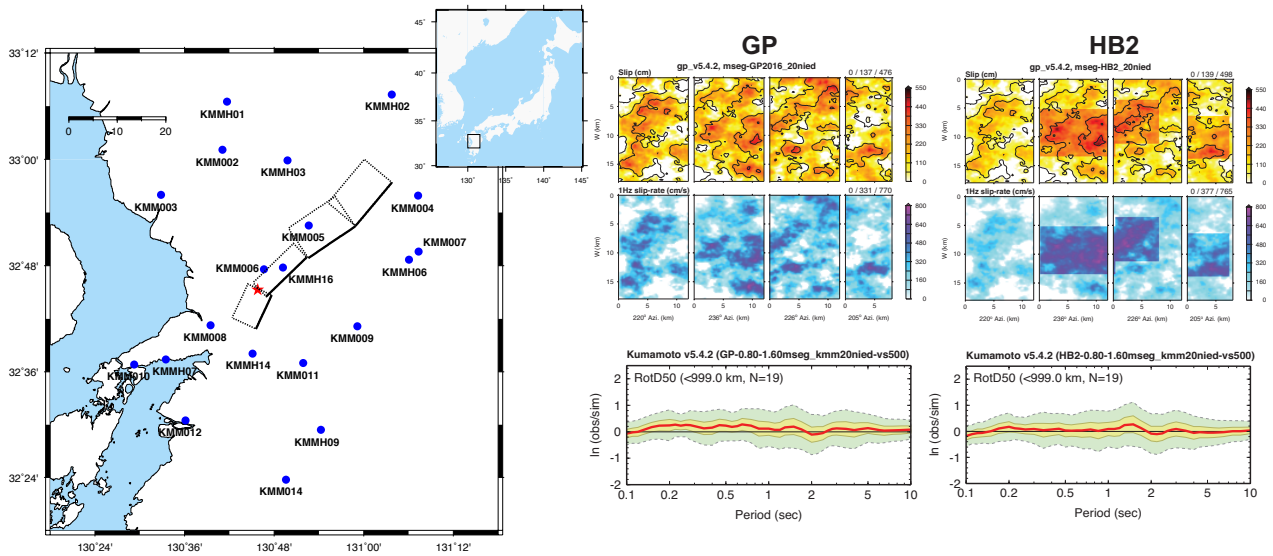

Fig. 9 - Left panel: Map of Kumamoto, Japan area showing the fault segments (dotted rectangles) used in simulations of strong ground motion from the M7, 2016 Kumamoto earthquake. Red star indicates the hypocenter location and blue dots indicate the strong motion stations location. Right panel: Rupture models and spectral acceleration goodness of fit, averaged over 19 stations used in ground motion simulations of the Kumamoto earthquake. Top panels: The first row shows the slip distributions and the second row shows the peak slip rate computed after low-pass filtering the source time function at 1 Hz. Isochrones indicate the rupture front at 1 s time intervals. Bottom panels: RotD50 horizontal spectral acceleration goodness of fit for the scenario earthquake simulations averaged over 19 stations generated with GP (left panel) and HB2 (right panel) ruptures. The goodness of fit is computed between the simulated and the recorded data [10].

7. Acknowledgements

This work was performed under the auspices of the U.S. Department of Energy by Lawrence Livermore National Laboratory under Contract DE-AC52-07NA27344, Release:LLNL-PROC-802920. It was partially supported by the Exascale Computing Project (ECP), Project Number: 17-SC-20-SC, and 2017 research project “Improvement for uncertainty of strong ground motion prediction” by the Nuclear Regulation Authority (NRA), Japan. All figures were made using Generic Mapping Tools (GMT) version 4.5.3 (http://www.soest.hawaii.edu/gmt) [11].

8. References

[1] Graves R, Pitarka A (2016): Kinematic ground motion simulations on rough faults including effects of 3D stochastic velocity perturbations, Bull Seis. Soc Am., 106, 2136–2153, doi: 10.1785/0120160088.

[2] Pitarka A (1999): 3D elastic finite-difference modeling of seismic motion using staggered grid with nonuniform spacing, Bull. Seis. Soc. Am. 89, 54–68.

[3] Dalguer LA, Day SM (2007): Staggered-grid split nodes method for spontaneous rupture simulation, J. Geophys. Res. 112, B02302, doi 10.1029/2006JB004467.

[4] Graves R, Pitarka, A (2010): Broadband ground-motion simulation using a hybrid approach. Bull. Seis. Soc. Am., 100(5A), 2095–2123. https://doi.org/ 10.1785/0120100057.

[5] Marone C, Scholz CH (1988): The depth of seismic faulting and the upper transition from stable to unstable slip regimes, Geophys. Res. Lett. 15, 621–624.

[6] Pitarka A, Dalguer LA, Day SM, Somerville P, Dan K (2009): Numerical study of ground-motion differences between buried- rupturing and surface-rupturing earthquakes. Bulletin of the Seismological Society of America, 99, 1521–1537.

[7] Dalguer LA, Miyake H, Day SM, Irikura K (2008): Surface-rupturing and buried dynamic rupture models calibrated with statistical observations of past earthquakes, Bull. Seis. Soc. Am. 98, 1147–1161.

[8] Dreger D,Wang K,Tinti E, Burgmann R,Taira T(2019): Rupture History of the July4 andJuly6 2019Ridgecrest Earthquakes, Abstract S31G-0494, 2019 AGU Fall Meeting.

[9] Ji C, Archuleta R, Tsuda K, Condon S (2019): Preliminary seismological analyses of 2019 Mw 6.4 Searles Valley and Mw 7.1 Ridgecrest California earthquakes, Abstract 259, 2019 SCEC Annual Meeting.

[10] Pitarka A, R. Graves, K.Irikura, K. Miyakoshi, and A. Rodgers (2019): Kinematic Rupture Modeling of Ground Motion from the M7 Kumamoto, Japan Earthquake, Pure App. Geophys., https://doi.org/10.1007/s00024-019-02220-5.

[11] Wessel P, Smith W (1998): New, improved version of generic mapping tools released, Eos Trans. AGU 79, 47, 579– 579, 10.1029/98EO00426.

